Received: 31 January 2022 | Revised: 5 May 2022 | Accepted: 6 May 2022

DOI: 10.1002/eqe.3668

RESEARCH ARTICLE

WILEY

# Risk-based seismic design of base-isolated structures with single surface friction sliders

**Gerard J. O'Reilly**[1,2] | **Hiroshi Yasumoto**[3] | **Yoshitaka Suzuki**[3] | **Gian Michele Calvi**[1,2] | **Masayoshi Nakashima**[3,4]

[1]Centre for Training and Research on Reduction of Seismic Risk (ROSE Centre), Scuola Universitaria Superiore IUSS di Pavia, Pavia, Italy

[2]European Centre for Training and Research in Earthquake Engineering (EUCENTRE), Pavia, Italy

[3]Kobori Research Complex (KRC), Kajima Corporation, Tokyo, Japan

[4]Disaster Prevention Research Institute, Kyoto University, Kyoto, Japan

**Correspondence**
Gerard J. O'Reilly, Centre for Training and Research on Reduction of Seismic Risk (ROSE Centre), Scuola Universitaria Superiore IUSS di Pavia, Pavia 27100, Italy.
Email: gerard.oreilly@iusspavia.it

**Funding information**
Italian Ministry of Education, University and Research

**Abstract**

Choosing friction pendulum isolators to avoid problems with device displacement capacity or boundary wall collision is a critical part of the seismic design of base isolation systems. This paper developed a probabilistic method to quantify the risk of failure in single friction pendulum bearing (FPB) devices. This was done by calibrating a demand-intensity model for FPBs from numerical analysis for several device property combinations. These properties encompassed the dynamic friction coefficient and effective radius of curvature—key parameters impacting these FPB devices' seismic response. Through this demand-intensity model, a closed-form and relatively simple approach to quantify the mean annual frequency of exceeding a given device displacement threshold, or risk of failure, was proposed. By applying this simplified method to several case study structures and comparing it with a more extensive assessment involving multiple stripe analysis (MSA) using hazard-consistent ground motions, the proposed simplified approach could provide very accurate estimates of displacement-based failure risk in FPB devices under the assumption of no non-linear behaviour in the superstructure. This proposed approach implies that structural engineers can now quickly assess the actual failure rates of different FPB device combinations used in practice to give a more uniform level of safety or reliability when designing and assessing FPB-isolated systems. It is also arguably much simpler, direct and accurate than currently available code-based approaches.

**KEYWORDS**
base isolation, friction pendulum isolators, risk, seismic design

## 1 | INTRODUCTION

Structural engineering applied in a seismic context typically involves designing and detailing a few dissipating elements in the overall lateral load-resisting system.[1] This can be achieved through the flexural yielding via plastic hinge formation in frame systems, bracing elements, more advanced technologies such as self-centring systems,[2] or active or semi-active control systems.[3,4] Base isolation is another technology whereby a part of the structure is segregated from the foundation via an isolation layer by placing the structural system upon a few special devices. It not only confines any dissipative action resulting from seismic shaking to the isolation layer but also modifies the modal properties of the overall structure

  

to significantly reduce floor accelerations and relative storey displacements transmitted to the superstructure. This has clear advantages in protecting and mitigating damage to structural and non-structural elements in the building, which are well-known sources of loss and potential disruption.[5,6]

Base isolation gained much popularity as a rubber-based elastomeric device, and its technology saw rapid development.[7] Various devices were studied and eventually applied in 1969 to a school building in Skopje, North Macedonia, as described in Naeim and Kelly,[8] among others. In the 1980s, a similar but different isolation system based on sliding was developed, termed a friction pendulum bearing (FPB)[9,10] and saw significant development.[11] It relies on the friction of a concave sliding surface to provide lateral resistance and a restoring force to the structure placed upon it. This was conceptually different to the elastomeric devices, which relied on the internal shear strains developed in the emulsified rubber system with the potential addition of a lead plug. Friction pendulum systems, and base isolation systems in general, have enjoyed great popularity in seismic engineering and have been applied to buildings, bridges, schools and hospitals, for example.[8,11]

For what concerns the seismic design provisions typically used to select and size base isolation devices, several codes of practice are in place worldwide. In particular, Eurocode 8[12] and EN15129[13] stipulate design and acceptance criteria be met for base-isolated structures in Europe, while the *Norme Tecniche per le Costruzioni*[14] provides a similar but more specific set of rules for application in Italy. ASCE/SEI 7–16[15] is used for design in the US, whereas NZSEE[16] provides guidance in New Zealand. Higashino and Okamoto[17] provide a comprehensive guide to the Japanese code of practice, with other studies like Pan et al.[18] and Becker et al.[19] also providing useful insight. Within these different guidelines and codes of practice worldwide, there is a common trend among all methods and procedures available for what concerns isolator device design. That is, they are generally based on the trial selection of devices using equivalent linear models and subsequent verification with dynamic analyses to check device performance (e.g., bearing displacement, uplift forces) and superstructure performance (e.g., storey drift, floor acceleration) criteria, typically following multiple design iterations.

While base isolation systems are perceived to offer superior performance, which has been demonstrated by Kitayama and Constantinou,[20] for example, design codes have been criticised for their relatively poor collapse performance in situations other than those they were specifically designed for, or when compared to other non-isolated systems.[21] In the case of FPBs, this generally relates to the exhaustion of the device's displacement capacity or collision with the surrounding moat wall, which can cause device failure or induce non-linear response in the superstructure. For example, studies like Kitayama and Constantinou[20] and Becker et al.[22] investigated the effect of displacement restraint in seismic isolation systems on the collapse performance of seismically isolated buildings and noted the key roles of displacement capacity or moat walls on the collapse performance. In particular, the probability of bearing failure was found in some cases[23] to be unacceptable due to excessive displacement demands that the isolators could not accommodate. Pant and Wijeyewickrema[24] investigated the effects of impact with boundary walls for seismic isolation systems considering different design levels and also near-fault ground motions. They found that if the isolation system impacts the boundary elements, it can be detrimental to the performance of the superstructure, especially at the ground storey level. A key observation of Erduran et al.[23] was that, when non-linearity occurs in the isolated superstructure, the ductility demand can often be larger than that of the corresponding fixed-base structure. Masroor and Mosqueda[25] also investigated the effects of superstructure flexibility. They noted that stiffer structures were more prone to structural collapse upon boundary wall impact, whereas more flexible structures were better able to absorb the impacts induced on them. These findings were also reflected in the work of Bao and Becker.[26] In addition to numerical studies, from observations following the 2016 Kumamoto earthquake in Japan, Takayama[27] reported how seismically isolated buildings performed well during the earthquake. However, the lack of consideration of detailing at the gap surrounding the buildings led to widely-observed damage to the non-structural elements installed at this location.[27]

Design codes in countries like Italy, the USA, Japan, and China do not provide specific limits for the distance between the structure and the moat wall. However, following consultation with several practitioners and academics in these countries, some general rules and typically encountered values were identified. In Japan, a value of 500 mm ±100 mm tends to be common for all devices and stems from the strain limits of rubber-based devices traditionally used. In China, a value no less than 1.2 times the displacement expected at the maximum considered earthquake is required. Considering the seismicity of an intensity eight zone, this would correspond roughly to a displacement limit of between 300 and 400 mm. In the US, this tends to be 400–500 mm for rubber-based devices and can reach up to 1 m for friction-based isolators due to their longer vibration periods. In Italy, the NTC 2018 requires that the distance should be able to accommodate the expected demands at the life safety limit state, which, when considering the seismicity of the region can result in displacements of between 100 and 300 mm. Thus, given the potentially detrimental consequences in the event of a moat wall collision and the range of limits specified in different countries, a design method to predict and limit the isolator displacement response that is compatible with different seismic regions' diverse needs is needed.

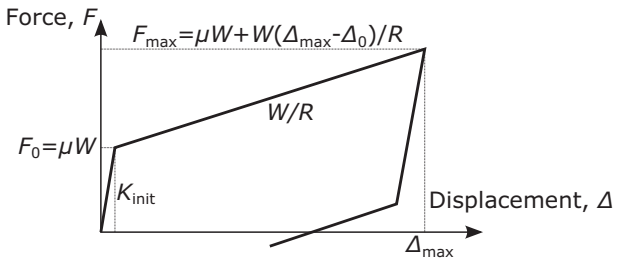


**FIGURE 1** Hysteretic behaviour of FPBs[9]

Performance requirements stipulated by codes are verified at few design intensities without a more comprehensive consideration of the uncertainty in hazard and structural response across all possible intensities, and they do not provide a robust quantification of the risk of device failure, as described by Cornell et al.[28] As argued recently by Kazantzi and Vamvatsikos,[29] clients requiring improved performance will generally find themselves designing for an increased seismic action (i.e., seismic shaking) when following code provisions but without any direct quantification of the actual increase in safety. Recent works[30,31] have focussed on providing additional bearing displacement capacity of between 1.5 and 1.8 times the code-specified demand value, in addition to shear strength requirements, to ensure a more reliable bearing response. Kazantzi and Vamvatsikos[29] have shown, however, that while these approaches are simple to implement in practice, again, their lack of consideration of the site's complete hazard curve and other response variability means that their ability to ensure accurate desired levels of safety is not guaranteed. As such, they are not entirely in line with what is generally known as modern performance-based earthquake engineering (PBEE).[32] As part of a comprehensive study on several building typologies and site hazards, Iervolino et al.[21] noted that isolated structures may have a worse collapse risk performance than non-isolated structures. These conclusions may be due to a seemingly conservative definition of collapse used for the bearing devices since other research[33] has shown that isolators can generally go far past the collapse displacement used in that previous study. However, more specific research that accounted for the failure mechanism in bearings by Kitayama and Constantinou[30] has also illustrated how minimum code-based designs for seismically isolated buildings in the US can have unacceptable collapse performance at the maximum considered earthquake intensity, which aligns with Iervolino et al.[21] Kitayama and Constantinou also show[20] that when examining the isolated structures via a detailed probabilistic assessment, the annual exceedance rates of storey drifts and floor accelerations prior to collapse are still lower than the corresponding non-isolated structure. These studies indicate the advantages offered by isolation but nonetheless, a better understanding of the collapse risk and how it may be handled in design warrants further research.

The above discussion highlights that while base isolation, and FPB systems, in particular, are capable of providing superior seismic performance in structures, the design approaches currently available do not offer a simple and comprehensive way to ensure adequate safety defined via risk and generally work on a trial-and-error basis in device selection. Erduran et al.[23] concluded that controlling or limiting the isolator displacement demands appeared to be an unsolved problem requiring new and creative approaches, and has also been recently discussed in Kazantzi and Vamvatsikos[29] also, for example. This article aims to propose such an approach and overcome these limitations noted above via a risk-consistent method with which FPB systems for any kind of structural typology can be sized. It capitalises on the mechanical properties of FPB devices and the closed-form risk solutions developed in recent years. It uses the PBEE framework outlined by Cornell and Krawinkler[34] as its basis and is conceptually similar to Kazantzi and Vamvatsikos[29] in its objectives. Through the specific FPB-oriented framework described herein, designers can target the seismic risk or safety they desire and identify suitable isolator bearings in a few simple steps before other necessary verification analyses are carried out. This minimises the number of trials and offers a more direct design approach that aligns with the risk-oriented objectives of modern PBEE.

## 2 | DEVELOPMENT OF DEMAND-INTENSITY MODELS FOR FPBS

### 2.1 | Characterising normalised FPB hysteretic behaviour

Consider a simple structure, whose vertical weight is $W$, sitting upon an isolation layer comprised of single FPBs. The FPB hysteretic behaviour can be described as shown in Figure 1.[9,10] In this model, which ignores initial stick-slip breakaway

effects, the initial lateral force required to move the FPB isolation system, $F_0$, is governed by the friction coefficient of its sliding surface, $\mu$, and the vertical weight acting on it, $W$. Once the isolators have been activated and the structure begins to slide horizontally on the FPBs, the structure's period of vibration, $T_{\text{iso}}$, is a function of the effective radius of curvature of the sliding surface, $R$, given by[8]:

$$T_{iso} = 2\pi\sqrt{\frac{R}{g}} \tag{1}$$

It is noted that past studies (e.g., Ref. 35) have shown the sliding stiffness of a single FPB isolator, denoted as $W/R$ in Figure 1, to also depend on the displacement amplitude. For large displacements, the stiffness is given by $W/Rcos\theta$, where $\theta$ is the rotation angle of the equivalent pendulum system at a given displacement.[9,10] For relatively small displacements, this $cos\theta$ term is approximately unity and Fenz and Constantinou[35] note that any resulting error is less than 5% when the displacement amplitude is less than $0.3R$; hence, it is omitted from the modelling procedure adopted herein.

In seismic design and assessment, it is typical to link the seismic response of a structure to a ground motion intensity measure (IM). The choice of an IM is mainly based on establishing a strong correlation (i.e., low dispersion) between the structural response and the IM values, amongst other issues. For non-isolated buildings, this is typically the spectral acceleration at the first mode period of vibration, $Sa(T_1)$. This is used in many methods, such as the equivalent lateral force method in Eurocode 8,[12] for example. Since the isolated building will vibrate in a first mode dominated response period of $T_{\text{iso}}$ once the FPB system has been activated, it appears logical to describe the IM as the spectral acceleration at that period, $Sa(T_{\text{iso}})$. Studies such as Mollaioli et al.[36] have investigated the use of different IMs for base-isolated buildings. An analysis of two case-study buildings found that peak ground velocity (PGV) tended to be a reasonable predictor of structure displacement demands, which was also noted in past works like Ryan and Chopra.[37,38] Different combinations of IMs may be used to minimise dispersion in seismic response prediction, with studies[39–44] investigating optimal IMs for assessing existing buildings. For base-isolated structures, $Sa(T_{\text{iso}})$ will be employed herein due to its simplicity and physical meaning. It has also been shown[36] to be a good predictor of isolated structures' response.

If the $Sa(T_{\text{iso}})$ of a single ground motion is linked with the resulting engineering demand parameter (EDP), a demand-intensity model is obtained and can be used as a simplified means to quantify seismic risk, as discussed in O'Reilly and Calvi,[45] among others. In the case of the FPB isolation systems described here, the EDP is the FPB device's lateral displacement, $\Delta$. If the force-displacement relationship of FPB systems described in Figure 1 is normalised by $W$, it can be noted that both $T_{\text{iso}}$ and the FPB backbone characteristics are independent of the building's properties; they are only a function of the effective radius curvature of the sliding surface, $R$, and its friction coefficient, $\mu$. Since this lateral resistance of the isolator bearing is essentially a function of $\mu$, a normalised intensity for a given ground motion can be defined as:

$$\rho = \frac{Sa\,(T_{iso})}{\mu} \tag{2}$$

What this means is that once the FPB isolation system is activated, the ground motion intensity required to reach a target displacement depends on the device's post-activation hardening ratio, which is a function of the effective curvature radius, $R$ (Figure 1). If both $\mu$ and $R$ are known, the FPB behaviour can be modelled and analysed with dynamic analysis using several ground motions. If this is done using non-linear dynamic analysis on many different isolator $\mu$ and $R$ combinations, then the normalised intensity required to reach a certain displacement, along with its uncertainty, are empirically quantifiable. Figure 2 illustrates a schematic representation of this, whereas Figure 3 plots an example of such an analysis for various isolators, described in detail in Section 2.3.

## 2.2 | Definition of demand-intensity model

A demand-intensity model reports the displacement demand of the FPB, $\Delta$, versus the normalised intensity, $\rho$. A linear representation in logspace is used here for the demand-intensity model, but it is noted that other formulations such as multilinear[46] and parabolic[47] may also suit specific contexts. This representation was commonly used and was the basis for the probabilistic seismic assessment procedure developed by Cornell et al.,[28] for example. It is particularly suited to systems with a first-mode dominated response without any strength or stiffness degradation, hence its suitability for the FPB systems examined here. Essentially, this linear model in logspace is given by:

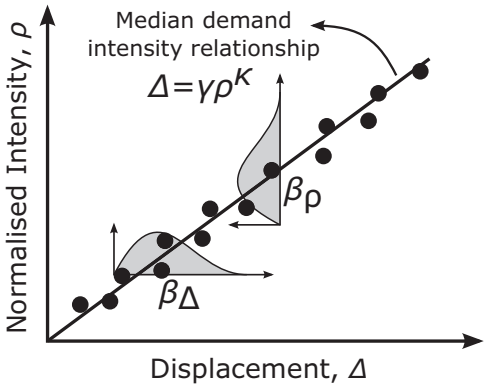


**FIGURE 2** Illustration of the demand-intensity model utilised for FPB isolator systems

$$\ln \Delta = \ln \gamma \ + \kappa \rho + \ln \epsilon_\Delta \tag{3}$$

where $\rho$ and $\Delta$ are the variables of interest, and $\gamma$ and $\kappa$ are fitting coefficients. The $\ln \varepsilon_\Delta$ term represents the error in the expression and is described by a standard normal distribution with a mean of zero and standard deviation $\beta_\Delta$, which denotes the dispersion in the displacement demand for a given intensity (Figure 2). It is often more useful, as will be seen in later sections, to instead know the dispersion in intensity required to exceed a given displacement threshold, which is denoted $\beta_\rho \approx \beta_\Delta/\kappa$ in Figure 2 and will be used herein. It is worth noting that this dispersion is assumed to be constant over the entire range of response considered (i.e., homoscedastic), which will be explored later.

Using the relationship described in Equation 3, the median demand-intensity model (i.e., $\ln \varepsilon_\Delta = 0$) can be simply described via a power-law, given as:

$$\Delta = \gamma \rho^{\kappa} \tag{4}$$

and will be the format used herein. This type of normalised demand-intensity relationship is equivalent to the $R$-$\mu$-$T$ relationships typically used for non-isolated buildings.[48–53] Instead, there is no ductility here per se but rather just an analogous response modification factor for a certain combination of device properties. Also worth noting is the physical significance of the $\gamma$ and $\kappa$ terms; $\gamma$ is essentially a fitting term but when $\kappa = 1.0$, it implies the equal-displacement rule typically adopted by building codes; however, when $\kappa > 1.0$, this means that the equal-displacement rule approximation no longer holds and its estimates of displacement response will be unconservative. These are herein denoted $\rho$-$\Delta$ curves and are assumed to be a function of just $\mu$ and $R$ of the FPB device. As will be seen through later application in Sections 3 and 4, this proposed formulation essentially replaces the equivalent linear methods employed by most design codes and guidelines worldwide[12,14–16] but operates under the assumption of an elastic superstructure response, which is discussed later. That is, instead of estimating the device displacement response from an overdamped design spectrum,[54] the response is computed directly from the ad-hoc demand-intensity models proposed here, which are specified as a function of actual FPB device characteristics. It is arguably more logical and accurate to use this direct probabilistic calibration that uses actual device response and accounts for FPB device response uncertainty instead of using the area-based equivalent viscous damping approaches[55] employing equivalent linear systems. This area-based damping approach[55] is well-known to be problematic[56,57] when applied to seismic response and often requires empirical calibration.[58–60] Hence, the demand-intensity models proposed here are essentially a rework of these existing methods except that the coefficients are directly derived based on numerical observations, and the equivalent linear system properties instead correspond to the device isolation period properties.

## 2.3 | Quantification of $\rho$-$\Delta$ curves for FPB devices

To quantify $\rho$-$\Delta$ curves for FPB systems, a vast set of analyses were carried out for isolators with different device properties. These were $R = [2.5, 3, 3.5, 4, 4.5, 5, 6, 7, 9]$ in metres and $\mu = [0.5, 1, 2, 3, 4, 5, 6, 7, 8, 9\ 10]$ in %, which represents isolators with vibration periods of $T_{\text{iso}} = [3.2, 3.5, 3.8, 4.0, 4.3, 4.5, 4.9, 5.3, 6.0]$ in seconds. These were selected to cover the full range

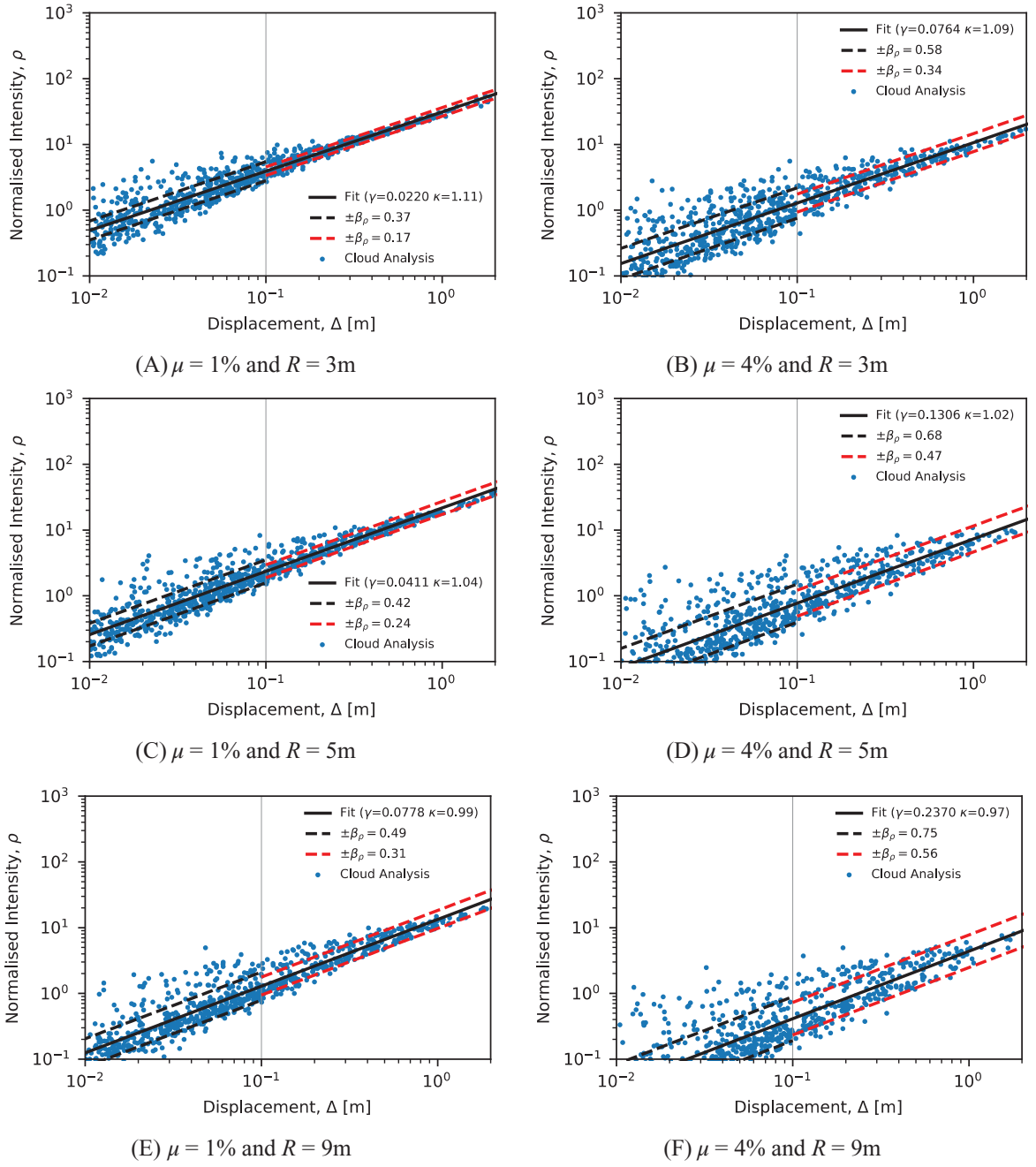


**FIGURE 3** Illustration of the cloud analysis on FPB systems with different device property combinations, reporting the relationship between normalised intensity and isolator displacement demand

of device property combinations that one may expect to encounter for FPBs in practice. However, practitioners must also pay close attention to device-specific guidelines regarding minimum stiffness criteria set out in building standards and also practical limitations regarding device dimensions when using the results presented here.

Each isolator bearing system was modelled as a single degree of freedom (SDOF) oscillator in OpenSees.[61] Since the response of the FPB isolation system is independent of the seismic weight, a nominal mass was assigned to the SDOF model. The bilinear model shown in Figure 1 was utilised to model the hysteretic behaviour; the yield force is the product of the friction coefficient considered and the seismic weight, and the hardening stiffness is the ratio of the seismic weight to the effective radius of curvature of the device being considered. This ignores the impact of large displacements on the hardening stiffness previously mentioned, whose influence on the results is discussed in later sections. It is worth noting that for the SDOF systems, the seismic weight and corresponding vertical force were modelled as constant during the

analysis. However, notable vertical axial force variations may result in individual FPBs during dynamic loading,[62] which alter the force-deformation of the individual device given its dependence on the actual vertical force transmitted through it. Hence, it is important to note that the SDOF oscillators used here are intended to represent an isolation system as a whole, whereby the net overturning moment of a building during dynamic response ensures that any increase in the vertical force on one isolator would mean a reduction for another device. This implies that the net force-displacement response of the isolation layer of the building remains constant and any axial force variation would not impact the lateral behaviour, as assumed here, although in-plane torsion and shear issues may arise in some instances.[62] Furthermore, issues such as accidental inclinations that can result during device construction and installation were not considered. Their impacts should be examined further in future work with sufficiently detailed modelling approaches.

The initial stiffness of the SDOFs was modelled as being very stiff with $K_{\text{init}} = 100{,}000$ kN/m. A sensitivity study showed this to be a reasonable value and did not impact the results or give numerical convergence issues. The bilinear hysteretic model did not consider the typically higher friction coefficient initially encountered in such devices that is required to initiate lateral sliding (i.e., the so-called stick-slip[11]). Also, the impacts of velocity, pressure and heating effects on the dynamic friction coefficient of the sliding surface were omitted. Work by Kumar et al.[63] noted that heating effects are an important factor in the numerical modelling of single friction pendulum surfaces, but pressure and velocity are less influential. Nevertheless, these are simplifying assumptions that may be checked and verified using more detailed numerical models that account for these once a suitable device combination has been identified using the design methodology described in Section 3. Lastly, no damping model was considered in the analysis aside from the hysteretic damping offered by the isolators themselves.

The SDOF models were analysed via cloud analysis[64] using a set of 200 ground motions selected from the NGA West2 database.[65] Cloud analysis involves using a large database of ground motions to examine structural response. Plotting the intensity of each ground motion versus the observed response forms a cloud of analysis results, as shown in Figure 3. All records were recorded on stiff soil and did not possess any near-fault directivity effects. Cloud analysis was chosen over other analysis methods like incremental dynamic analysis[66] to avoid any bias issues due to excessive scaling of ground motion records, as recently noted by Dávalos and Miranda,[67] among others. Other methods like multiple stripe analysis (MSA)[68] may have been used, but since the objective was not to accurately characterise the site hazard of one location but rather to develop a general demand-intensity model, cloud analysis was deemed a more suitable choice. The ground motions were also scaled up by two to ensure a sufficient number of response cases with relatively large displacement demand (i.e., $\Delta > 1$ m) were observed. These were needed to fit the demand-intensity model over the entire range of potential isolator responses, but their scaling was limited to minimise any significant biasing impact on the results.

Figure 3 shows the response results obtained for the different FPB isolator combinations considered, plotting the normalised intensity $\rho$ versus the isolator demand $\Delta$. By representing the results in logspace, it is clear that there is indeed a linear trend between the FPB isolator displacement and the normalised intensity required to exceed it, validating the choice of the demand-intensity model in Equation 4. Performing a least-squares regression fit of the adopted demand-intensity model shows the median trend in solid black matching the cloud analysis data well in Figure 3. Also illustrated are the dispersion bounds plotted with dashed lines around the median, representing $\beta_\rho$. It can be noted that the scatter around the median begins to reduce with increased demand, suggesting that the assumption of constant dispersion at all levels of demand may not be entirely representative but rather a mathematical convenience. This is a somewhat expected result and is not unique to isolation systems, as it has been widely observed for ductile moment and braced-frame systems in the past. It can be associated with the stabilisation of the structural system within a set inelastic mechanism in traditional non-isolated systems. For this reason, segregation was made between the two dispersions plotted for a displacement of $\Delta > 0.1$ m and below, where the dispersion of points $< 0.1$ m is shown via the dashed black line and the dashed red line represents the dispersion of points $> 0.1$ m. This choice was made to have a more representative quantification of the dispersion with respect to the demand-intensity model at displacements of interest in seismic design and not to have the uncertainty unnecessarily amplified by scatter at lower displacements that may not be of engineering interest.

## 2.4 | Fitting of $\rho$-$\Delta$ curves for FPB devices

The previous sections described the analysis of different FPB isolator combinations to characterise their seismic behaviour via $\rho$-$\Delta$ curves. It was seen in Figure 3 how the results obtained indicated that the logspace linear demand-intensity model described in Equation 4 was suitable to describe their seismic response. This section will look to fit empirical relationships to these results such that the $\rho$-$\Delta$ curves of FPB devices can be directly estimated by knowing just the FPB device

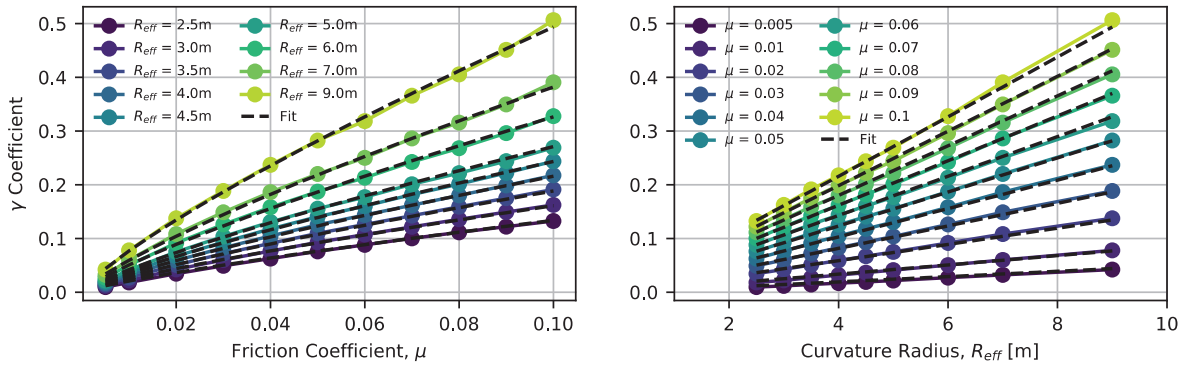


(A) $\gamma$ fitting with Equation 5

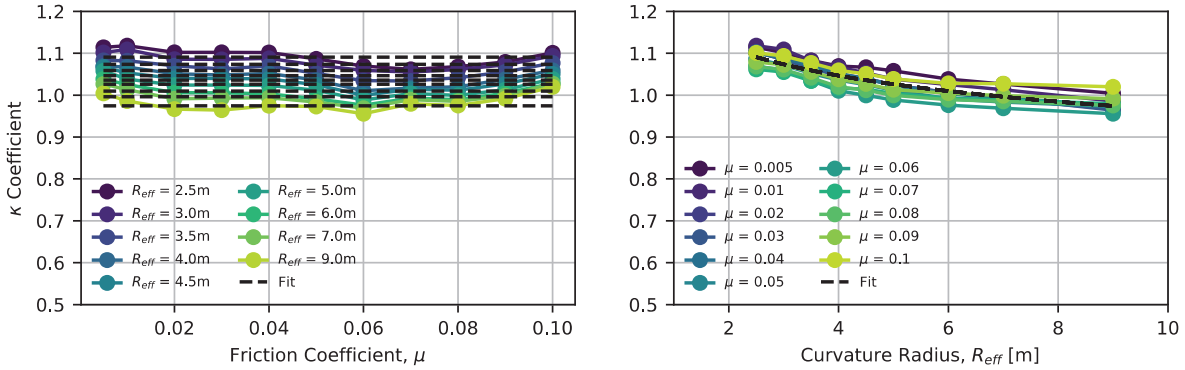


(B) $\kappa$ fitting with Equation 6

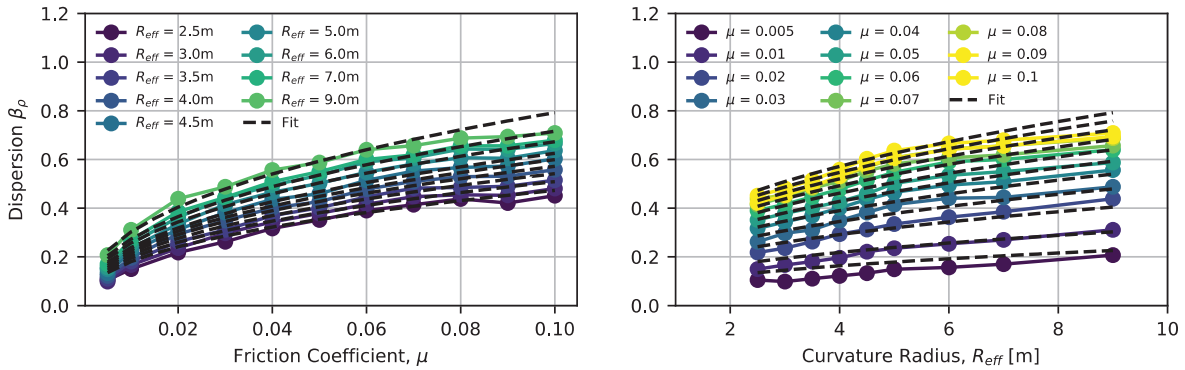


(C) $\beta_\rho$ fitting with Equation 7

**FIGURE 4** Illustration of the coefficients derived from cloud analysis and two-step regression

properties. It is anticipated that the results of the empirical fitting presented here are used by practitioners in future for the preliminary design of FPB isolators. Additional research may look to repeat such analysis and investigate some of the modelling assumptions made here.

The approach adopted herein was via two-step regression. That is, the coefficients required for the median demand-intensity model (i.e., $\gamma$ and $\kappa$) were fitted for each combination in the first step. In the second, these coefficients were then fitted with relationships that directly link them to the device properties $\mu$ and $R$. The first step of the regression has already been performed for each FPB device in Section 2.3, with the fitted $\gamma$ and $\kappa$ parameters included in the subplot legends of Figure 3, for example. Figure 4 plots the results of the first step of the regression for all FPB device combinations, whereby the $\gamma$ and $\kappa$ terms are plotted against the device properties. Clear trends for the coefficients can be observed in both cases. Figure 4A shows that both $\mu$ and $R$ have a notable influence on the $\gamma$ term. Figure 4B shows that just $R$ impacts the $\kappa$ term, with $\mu$ having no significant influence for the isolators examined.

The second step was to identify a suitable model for these coefficients in Figure 4. Given the aforementioned observations, a power-law relationship was again found to be most representative and is described by:

$$\gamma = a_1 \mu^{b_1} R^{c_1} \tag{5}$$

$$\kappa = a_2 R^{c_2} \tag{6}$$

By performing a least-squares regression with the data in Figure 4A,B, suitable coefficients were found to be $a_1 = 0.337$, $b_1 = 0.808$, $c_1 = 1.02$, $a_2 = 1.183$, $c_2 = -0.088$ for $R$ and $\mu$, respectively. These fitted relationships are also plotted in Figure 4. A good match is observed between the actual data derived from the demand-intensity models from cloud analysis and the proposed models described here.

Likewise for the dispersion $\beta_\rho$, the trends versus both $R$ and $\mu$ are plotted in Figure 4C. Again, it can be seen that the trends could be represented by a power-law fit described as:

$$\beta_\rho = a_3 \mu^{b_3} R^{c_3} \tag{7}$$

which when fitting to the data, the coefficients were identified as $a_3 = 0.857$, $b_3 = 0.418$, $c_3 = 0.403$. The fitting is generally not as refined when compared to other parameters fitted in Figure 4A,B. Nonetheless, this relationship represents the dispersion around the demand-intensity model associated with the record-to-record variability only. It does not represent the additional device-based uncertainties that may impact the seismic response. Issues like the impact of heating and velocity could be incorporated by simply amplifying the dispersion value $\beta_\rho$ artificially instead of more specific analyses, as is done for the response analysis of buildings in guidelines like FEMA P695[69] or FEMA P-58,[70] or in Kitayama and Constantinou[71] for isolated buildings, for example. Furthermore, the impacts of device friction coefficient variability could be investigated by varying the input values for the expressions developed here and examining the outcome. Experimental data like that examined by Barone et al.[72] could also prove useful in such situations since the variability observed from tests could be directly incorporated. Furthermore, the impact of large displacement demand on the hardening stiffness in the devices may be investigated in the context presented here. As previously mentioned, this was not considered here to maintain a degree of simplicity in the approach proposed in the next section. However, it is noted that its omittance is a conservative assumption for what concerns displacement demands in the bearings. Worth noting also is that the relationship and coefficients plotted in Figure 4C are fitted to the dispersion in the demand-intensity model for demands of $\Delta > 0.1$ m and above only, which would correspond to the black dashed lines in Figure 3.

## 3 | A RISK-BASED APPROACH TO FPB SYSTEM DESIGN

The goal here is to develop a risk-based design approach for FPB-isolated systems. There are two important parts needed to estimate the risk: the seismic hazard at the site of interest and the seismic vulnerability of the structural system.

The first part reflects the information computed via probabilistic seismic hazard analysis (PSHA), where the rate of exceeding a given level of intensity over a specified period may be computed. The second part then represents the probability of exceeding a displacement threshold for such a given intensity level, termed the seismic fragility function. When integrated, these parameters describe the risk of a given displacement threshold being exceeded. It can be probabilistically quantified using the mean annual frequency of exceedance (MAFE), $\lambda_\Delta$, by integrating the probability of failure for a chosen IM, $P[\Delta > \Delta_{\text{lim}} | IM = s]$, with the site hazard curve, $H(s)$, as follows:

$$\lambda_\Delta = \int_0^{+\infty} P[\Delta > \Delta_{lim} | IM = s] \, |dH(s)| \tag{8}$$

In the specific case of FPB-isolated systems, a site's hazard curve $H(s)$ can be computed for the IM in question. This is $s = Sa(T_{\text{iso}})$ for a given device $R$. If the performance, or limit state of interest, in an FPB isolator system is taken as the exceedance of a given isolator displacement threshold limit, $\Delta_{\text{lim}}$, then the probability of exceeding it for a given intensity $P[\Delta > \Delta_{\text{lim}} | IM = Sa(T_{\text{iso}})]$ is described by the $\rho$-$\Delta$ curves developed in Section 2. This means that a designer can use the curves calibrated previously to compute the risk of failure $\lambda_\Delta$ for a given isolator displacement, $\Delta$, if $\mu$ and $R$ are known and

the superstructure is expected to remain elastic. This may also be rephrased: for a target MAFE and maximum displacement, suitable device combinations of $\mu$ and $R$ can be identified. For example, if a designer has limitations on the possible value of $\mu$ because of the sliding surface materials available to the device manufacturer, they can check which value of $R$ would satisfy the design requirements. This formulation in a simplified and practice-oriented manner is presented below alongside an example implementation.

As mentioned, the first requirement to implement such a methodology is a site hazard curve at the IM of interest for the isolation system. As mentioned previously, the IM considered here is the spectral acceleration at the isolation period of the FPB system, $Sa(T_{\text{iso}})$. Therefore, from PSHA, its hazard curve may be computed and is denoted as $H(s)$, representing the mean annual frequency of exceeding a ground shaking level of $Sa(T_{\text{iso}}) = s$. Equation 8 represents the general formulation of the PEER PBEE methodology,[34] where the MAFE is estimated by integrating the seismic fragility with the associated hazard. With a view to a more practice-oriented approach, Cornell et al.[28] derived a closed-form expression that could be easily used, whereby engineers would make use of power-law fit to the hazard curve and also capitalise on the linearity of the demand-intensity model in logspace. Vamvatsikos[73] furthered this approach by extending the hazard model fit to a second-order model given by:

$$H(s) = k_0 \exp\left(-k_1 \ln s - k_2 \ln^2 s\right) \tag{9}$$

where $k_0$, $k_1$ and $k_2$ are the site hazard curve fitting coefficients obtained by simply fitting the expression to the hazard curve calculated in PSHA. With this refined hazard, the closed-form expressions proposed by Cornell et al.[28] to estimate the MAFE were rederived and proposed as:

$$\lambda_{\Delta} = \sqrt{p}\, k_0^{1-p} [H(s)]^p \exp\left(0.5 p k_1^2 \beta_{\rho}^2\right) \tag{10}$$

$$p = \frac{1}{1 + 2k_2\beta_{\rho}^2} \tag{11}$$

This essentially means if the hazard curve parameters are known, and the median seismic intensity required to exceed a displacement threshold limit is known along with its associated uncertainty, then the MAFE, or risk of failure, can be simply computed using Equation 10. Figure 5 illustrates a step-by-step implementation of the proposed procedure.

## 4 | CASE STUDY APPLICATION

### 4.1 | Simplified evaluation via proposed approach

Using the risk-based approach outlined in Section 3, the seismic performance of an FPB isolation system may be evaluated via a case study example. This is termed evaluation since the process involves a trial-and-error approach, but given its expedited nature, it can easily be utilised in a design situation to trial a certain isolation system's suitability before detailed verification analysis.

For a building located in L'Aquila, Italy, the MAFE of exceeding an FPB displacement threshold of $\Delta_{\text{lim}} = 0.4$ m is determined for an FPB isolation system comprising $\mu = 3\%$ and $R = 4$ m isolators. This information encompasses Steps 1–3 outlined in Figure 5. The following text will discuss the rest of the steps required to compute the MAFE, which will be confirmed via extensive verification analysis in the next section.

Step 4 is the identification of the seismic hazard. Since the isolator bearings are $R = 4$ m and the ground motion IM is $Sa(T_{\text{iso}})$, the period of vibration was computed as $T_{\text{iso}} = 4.01$s using Equation 1. With $T_{\text{iso}}$ known, the seismic hazard curve was identified (Step 5) for L'Aquila using the SHARE hazard model[74] by performing a PSHA for $Sa(T_{\text{iso}} = 4.01\text{s})$ using the OpenQuake engine[75] and the results are shown in Figure 6. Also shown are the hazard curves corresponding to other periods of vibration that may be investigated for other FPB isolator radii. Utilising the second-order seismic hazard model fit in Equation 9, the coefficients for $Sa(T_{\text{iso}} = 4.01\text{s})$ are $k_0 = 8.18 \times 10^{-7}$, $k_1 = 2.976$ and $k_2 = 0.186$ (Step 5).

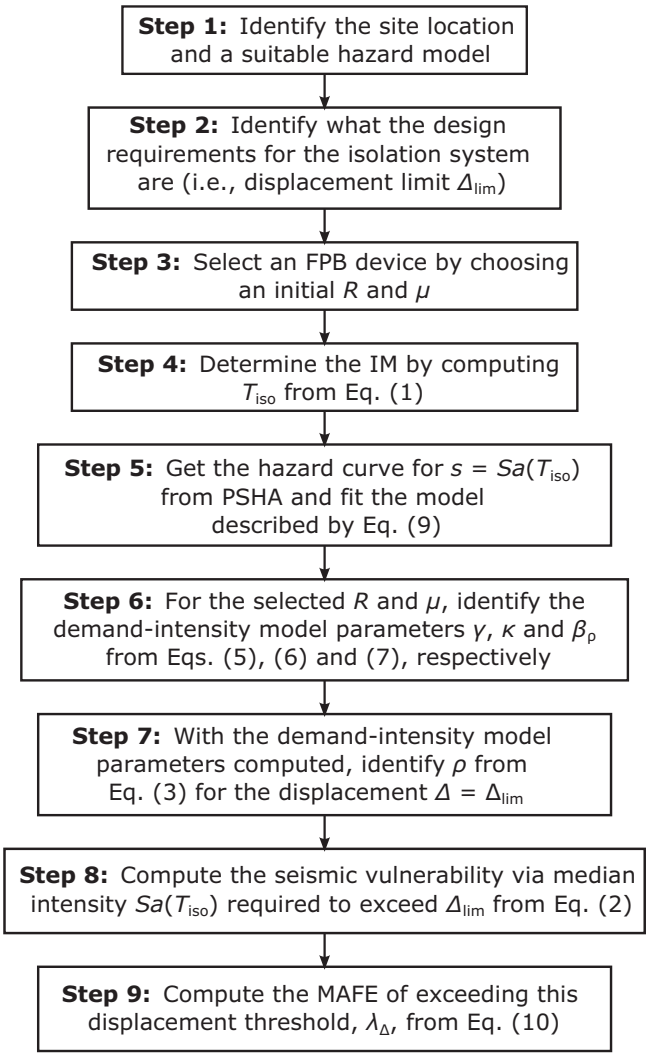


**FIGURE 5** Step-by-step implementation of the proposed procedure

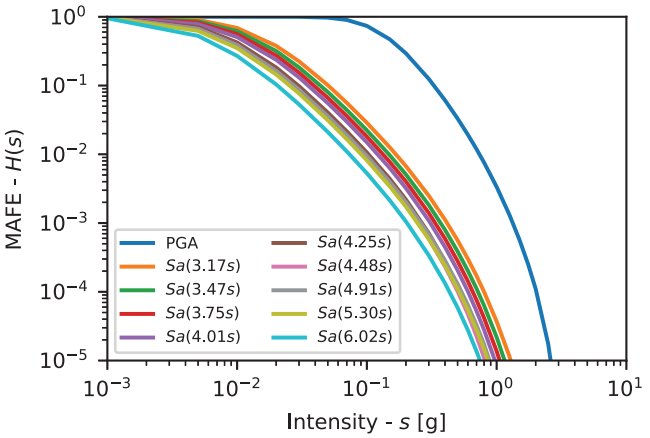


**FIGURE 6** Mean hazard curves computed for a site in L'Aquila, Italy located at Longitude: 13.3995 Latitude: 42.3498 with a soil type of $V_{s30}$ = 360 m/s, corresponding to stiff soil[12]

Using the site hazard and candidate FPB isolator properties, the approach described in Section 3 was implemented to estimate the MAFE of the target displacement threshold of $\Delta_{\text{lim}} = 0.4$ m. From the $\rho$-$\Delta$ curves developed in Section 2.4, the demand-intensity model coefficients and associated dispersion were computed in Step 6 as:

$$\gamma = a_1 \mu^{b_1} R^{c_1} = 0.337(0.03)^{0.808} (4.0)^{1.02} = 0.08 \tag{12}$$

$$\kappa = a_2 R^{c_2} = 1.183 (4.0)^{-0.088} = 1.05 \tag{13}$$

$$\beta_\rho = a_3 \mu^{b_3} R^{c_3} = 0.857(0.03)^{0.418} (4.0)^{0.403} = 0.35 \tag{14}$$

Knowing the displacement threshold and the demand-intensity model parameters, the median seismic intensity to exceed $\Delta_{\text{lim}} = 0.4$ m is computed in Step 7 and 8 as:

$$\rho = \left(\frac{\Delta}{\gamma}\right)^{\frac{1}{\kappa}} = \left(\frac{0.4}{0.08}\right)^{\frac{1}{1.05}} = 4.57 \tag{15}$$

$$Sa\ (T_{iso}) = \rho\mu = 4.57\ (0.03) = 0.137g \tag{16}$$

Knowing this median intensity and the dispersion value, the MAFE can be computed in Step 9 as:

$$\begin{aligned} \lambda_\Delta &= \sqrt{p}\, k_0^{1-p} [H(s)]^p \exp\left(0.5 p k_1^2 \beta_\rho^2\right) \\ &= \sqrt{0.96} \left(8.18 \times 10^{-7}\right)^{1-0.96} \left[1.45 \times 10^{-4}\right]^{0.96} \exp\left[0.5 (0.96) (2.976)^2 (0.35)^2\right] \\ \lambda_\Delta &= 1.895 \times 10^{-4} \end{aligned} \tag{17}$$

where:

$$p = \frac{1}{1 + 2k_2\beta_\rho^2} = \frac{1}{1 + 2(0.186)(0.35)^2} = 0.96 \tag{18}$$

$$\begin{aligned} H(s) &= k_0 \exp\left(-k_1 \ln s - k_2 \ln^2 s\right) \\ &= 8.18 \times 10^{-7} \times \exp\left(-2.976 \times \ln 0.137 - 0.186 \times \ln^2 0.137\right) \\ &= 1.45 \times 10^{-4} \end{aligned} \tag{19}$$

This value of MAFE for the given FPB isolator type and displacement threshold can be plotted as shown in Figure 7 via the red crosses. If the same exercise described above is repeated for many combinations of FPB isolator properties and displacement thresholds, the demand-hazard curves shown in Figure 7 can be generated quite easily. This would simply involve obtaining the site hazard curves corresponding to the different FPB effective curvature radii, which were shown in Figure 6. Once obtained, the demand-hazard curves are easily computed by following the relatively simple calculations outlined. These were computed for a range of FPB isolator types and displacement threshold and are plotted in two different ways: Figure 7(left) highlights the impact on the MAFE for a given $\mu$ and different $R$ values, whereas Figure 7(right) shows the impact of $\mu$ for a given value of $R$. It can be seen how in order to reduce the $\lambda_\Delta$ below a certain threshold, a designer would need to either decrease the $R$ or increase the $\mu$.

With such a set of demand-hazard curves, a designer may clearly see what the risk-based performance of any such FPB isolation system would be and verify if the chosen system matches their performance requirements. That is, for a given FPB isolator, such as the combination calculated above and plotted via the red cross in Figure 7, a designer may evaluate whether the MAFE of exceeding the displacement threshold of 0.4 m is equal to $\lambda_\Delta = 1.895 \times 10^{-4}$, which would correspond to a return period of 5276 years, is sufficiently low. This displacement threshold may correspond to the FPB

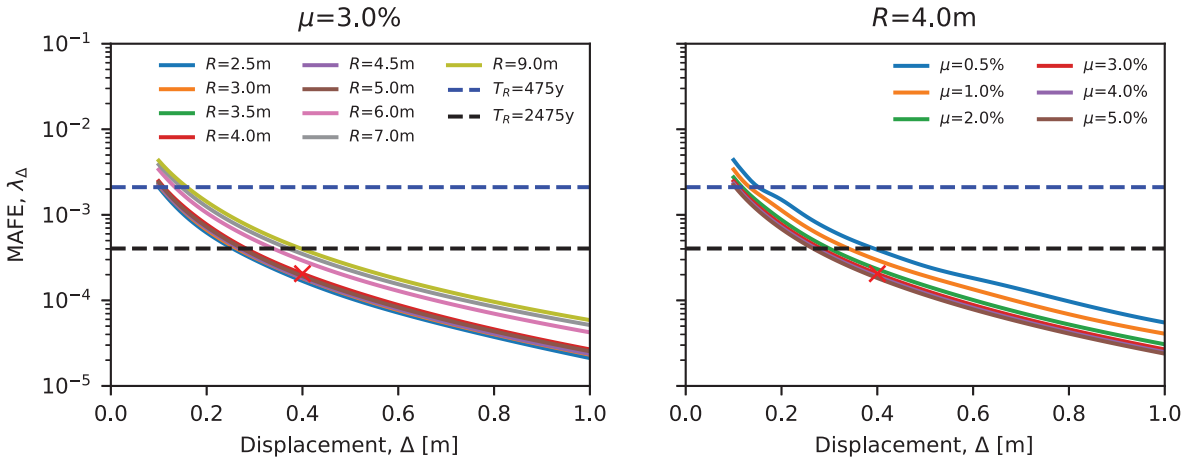


**FIGURE 7** Demand-hazard curve for a range of FPB isolator combination types located in L'Aquila, Italy, where the curves (left) are for a fixed value of $\mu$ whereas (right) is for a fixed $R$

device's displacement capacity or the distance between the building's base slab and the moat wall, which are limited to prevent collision or pounding, or damage to piping or other elements that bridge the isolation layer, which has been observed during the Kumamoto and Tohoku earthquakes in Japan.[27]

Likewise, for a given displacement threshold and target MAFE, a designer may compute these demand-hazard curves and determine a feasible FPB isolator combination. For example, if a designer wanted to ensure a displacement threshold of 0.3 m with a return period of 2475 years, Figure 7 shows that only FPB isolators with $R < 6$ m and $\mu > 3\%$ would suffice. However, it is recalled that the proposed method relies on the assumption of an elastic superstructure; for such return periods, this assumption would need to be verified as some non-linearity in the superstructure may arise at these intensities. For a less restrictive return period of 475 years, on the other hand, it is clear that all isolation systems would satisfy the performance objectives for a displacement threshold of 0.3 m. Instead for a much more restrictive return period of 5000 years and a displacement threshold of 0.3 m, Figure 7 shows that none of the FPB isolators would be suitable and some other supplemental system would be needed.

As a check, if instead of utilising the closed-form expression in Equation 17 and the demand-intensity model is directly integrated with the seismic hazard curve according to Equation 8 via the trapezoidal rule, the resulting MAFE is $\lambda_\Delta = 2.051 \times 10^{-4}$, which is herein termed the "exact" value, whereas $\lambda_\Delta = 1.895 \times 10^{-4}$ and is termed the "approximate" value computed previously. It can be seen that these two values are very similar and thus the closed-form expression to estimate the MAFE is suitable for the purposes described here.

## 4.2 | Verification analyses

What is interesting to note is that the results presented in Figure 7 were generated without any knowledge of the building system that will be placed upon the FPB isolation system. In theory, it should be possible to construct various types of building using the results presented here for the site in L'Aquila, provided that the superstructure undergoes little to no inelasticity. This assumption of an elastic superstructure is important to bear in mind depending on the building code adopted for the complete building verification. In particular, ASCE 7–16[15] allows some non-linearity in the superstructure meaning that the proposed approach should be used with care and its results verified using non-linear dynamic analysis accounting for possible superstructure non-linearity. However, other codes like Eurocode 8,[12] the Italian building code[14] and the New Zealand guidelines[16] recommend the modelling the superstructure as elastic, meaning the assumptions used herein are reasonable, although these codes do in some cases allow for some slight non-linear superstructure behaviour.

This section aims to trial different systems with a different number of storeys and structural systems to see whether, for a given isolation system and displacement threshold, the values of MAFE computed in Section 4.1 can be verified via extensive dynamic analyses. This was done using four simple case study buildings, comprising both single storey and six-storey structures, in addition to flexible moment-resisting frame (MRF) system and a much stiffer dual MRF and

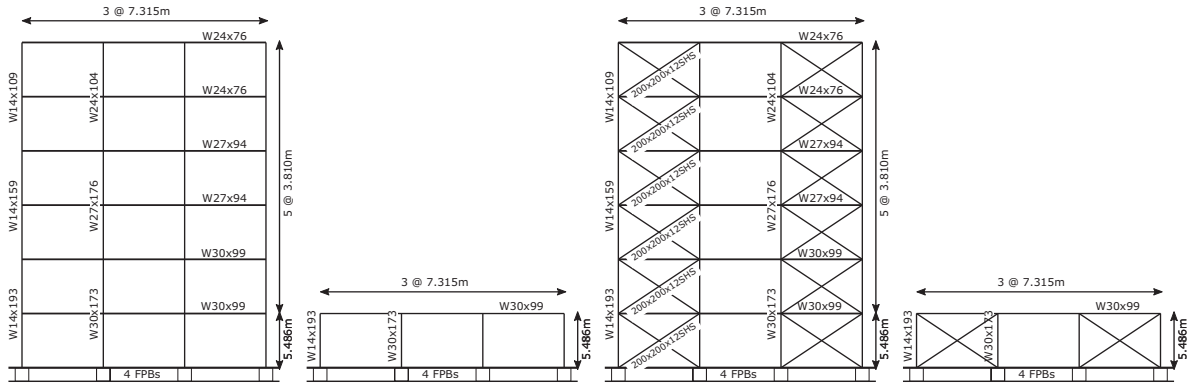


**FIGURE 8** Illustration of the case study steel frame buildings

**TABLE 1** Modal properties of the case study steel frame buildings

| | MRF | | CBF | |
|---|---|---|---|---|
| | 1 storey | 6 storey | 1 storey | 6 storey |
| $T_1$ [s] | 0.36 | 1.36 | 0.26 | 0.58 |
| $M_1$ [%] | 73.7 | 72.8 | 99.1 | 91.8 |
| $T_{iso}$ [s] | 4.00 | 4.13 | 4.00 | 4.00 |
| $M_{iso}$ [%] | 99.9 | 99.7 | 99.9 | 99.9 |

concentrically-braced frame (CBF) system. These were evaluated assuming the FPB isolation system of $R = 4$ m and $\mu = 3\%$ using the site hazard of L'Aquila.

The building systems comprised a single storey and a six-storey steel MRF structure, whose design is described in Tsai and Popov.[76] Figure 8 illustrates the salient features of the buildings. Different configurations (i.e., short versus medium height and stiff versus flexible) were hypothesised to quickly examine any potential impacts on the MAFE for the isolators. To do this, the first storey of the six-storey building was simply modelled to create the single-storey structure and, in both cases, diagonal concentric braces with a square hollow section of 200 × 200 × 12SHS were added. Numerical models of each building were developed in OpenSees. The structural members were modelled as elastic frame elements and the brace members modelled as truss elements; therefore, not anticipated to undergo any inelastic response. Table 1 lists the modal properties of both fixed-base and isolated buildings, where $M_1$ is the percent of mass participating in the first mode of the fixed-base structure, $T_{iso}$ is the isolated building's period and $M_{iso}$ is the percent of mass participating in the first isolated mode. $T_{iso}$ and $M_{iso}$ were obtained by setting the stiffness of the isolator bearings to the post-activation sliding stiffness to mimic their behaviour once activated. Overall, it can be seen that the models are representative of low- to mid-rise structures with fixed-base periods ranging from 0.26s to 1.36s, and examining their fundamental mode's displacement profile shows no stiffness irregularities along their height. Table 1 also shows how the $T_{iso}$ of each building is equal to the expected value of $T_{iso} = 4$s, except the six storey MRF, whose superstructure flexibility has a slight impact. It is interesting to note that this follows a rule-of-thumb used in Japan where if the corresponding fixed-base building's period is at least four times shorter than the isolated period, the superstructure's flexibility will not impact the isolated structure's response. Here, the fixed-base structure would need to have a period less than 1s ( = 4.0s/4) to not be affected, which is violated only for the six storey MRF structure, which consequently has a slightly longer $T_{iso}$. What this means is that the response of each structure is dominated by the first isolated mode and no significant contribution is anticipated from the second mode response of the superstructure. When this second mode becomes significant, it may result in both higher and lower isolator displacement demands due to the increased participation and contribution of the second mode to the overall response, which would effectively increase the dispersion in the fragility function. Care should be taken when dealing with taller structures outside the period range examined here and when the fundamental mode is no longer dominant. Future work on a larger set of structures may investigate this potential contribution and its magnitude in the context of the work presented here but readers interested in how higher mode contributions may be considered are referred to Priestley et al.[57] for further details.

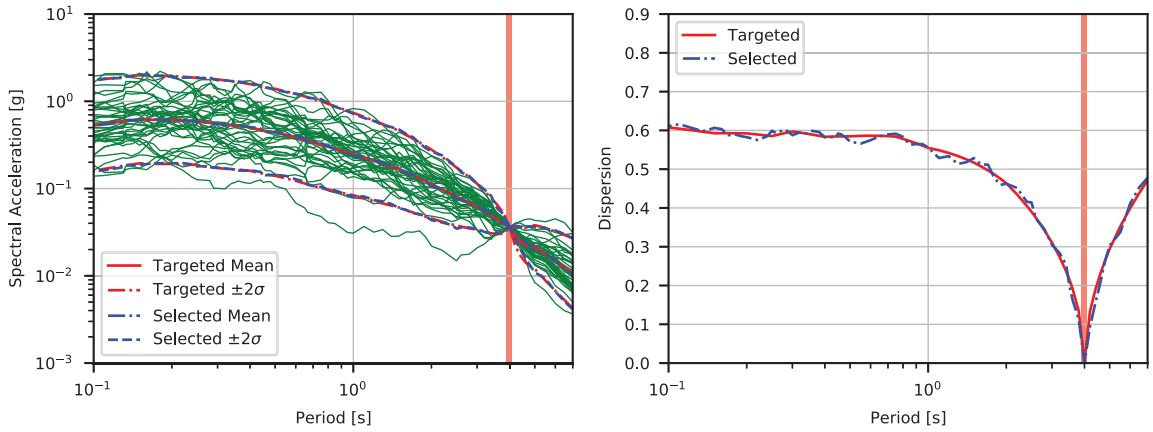


**FIGURE 9** Illustration of the ground motions selected via the CS method for $Sa(T_{iso} = 4.0s)$ at the case study site in L'Aquila for a 10% probability of exceedance in 50 years. (A) FPB isolator displacements at each MSA stripe for the 6 storey MRF structure. (B) Fragility functions for $\Delta_{lim} = 0.4$ m exceedance estimated via the simplified procedure. (C) Comparison of the computed MAFE for each case study

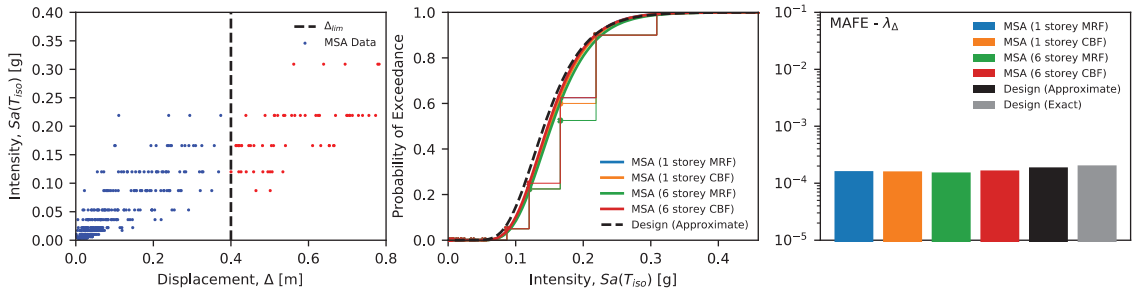


(A) FPB isolator displacements at each MSA stripe for the 6 storey MRF structure

(B) Fragility functions for $\Delta_{lim} = 0.4$m exceedance estimated via the simplified procedure

(C) Comparison of the computed MAFE for each case study

**FIGURE 10** Illustration of the risk analysis results

The FPB isolators were modelled using *zeroLength* elements in OpenSees, whose hysteretic behaviour followed that illustrated in Figure 1, where isolator failure or collision with an exterior moat wall was not explicitly modelled and no damping was modelled in these elements. Impacts of stick-slip breakaway and friction coefficient variation with velocity and pressure were also not modelled.

To evaluate the seismic risk of these structures rigorously, MSA[68] was used. This involved 40 ground motion records being selected and scaled to match the seismic hazard disaggregation at several intensities via the conditional spectrum (CS) method.[77] In this study, the same PSHA results were used and the CS was generated for several intensities ranging from a 90% to 0.01% probability of exceedance in 50 years, which represent a return period range of 22–4975 years. Ground motion records were selected and scaled to match this conditional distribution and an example is shown in Figure 9. It can be seen how the mean and distribution of the selected records matched the target hazard quite well.

With ground motion records selected and scaled to represent the seismic hazard at several intensities, the MSA was run and the response of each case study building configuration was obtained. The EDP used in the analyses was the maximum displacement of the FPB isolation system, so the displacement demand at the FPB isolation layer was known for multiple ground motions at several intensities, as shown in Figure 10A. To estimate the seismic fragility, the number of displacement threshold exceedances at each MSA stripe were counted as a fraction of the analyses run. That is, for the $\Delta_{lim} = 0.4$ m displacement threshold, the number of exceedances divided by the number of ground motions per intensity stripe would correspond to the probability of exceedance. Figure 10B plots the empirical cumulative distribution function of these fractions versus the intensities at which they were observed via the stepped lines. If a lognormal distribution is assumed, the maximum likelihood method can be used to fit fragility functions. These continuous fragility functions are also plotted in Figure 10B via the smooth lines, where it can be seen that the median intensity is very similar for each

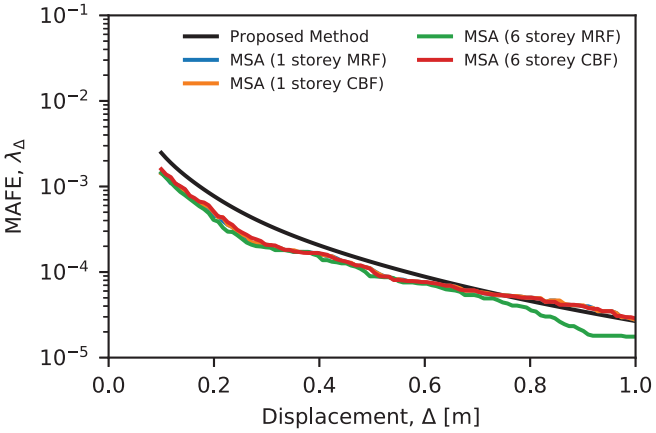


**FIGURE 11** Demand-hazard curves for each case study building where the MAFE computed from MSA are compared to the proposed simplified procedure

structure. Furthermore, this median value also corresponds well to that estimated using the proposed approach in Step 8 using Equation 16, indicating that it is indeed representative of different kinds of structures. The dispersion values were observed to be 0.30–0.31, which also match the empirical value of $\beta_\rho = 0.35$ computed in Step 6 via Equation 14. Again, this dispersion represents the uncertainty associated with record-to-record variability only. Other sources of uncertainty could also be considered, as is typically done for other building typologies.[78–80] Further work should be conducted to give guidance on the anticipated values and sources of dispersion that should be used in practice for different structural typologies.

By taking these fragility functions generated for each case-study building via MSA and integrating them with the seismic hazard curve shown in Figure 6, the MAFE was computed. These are plotted in Figure 10C for each case, which vary between 1.55 and $1.67 \times 10^{-4}$ along with the approximate and exact MAFEs calculated in Section 4.1, which were $1.895 \times 10^{-4}$ and $2.051 \times 10^{-4}$, respectively. There is a very slight and conservative overestimation of the MAFE through the simplified method. However, two important findings are clear. The first is that the seismic risk of exceeding the $\Delta_{\text{lim}}$ displacement threshold is independent of the structural typology placed upon the isolation layer, though it must be stressed that this is provided the superstructure remains elastic and is first-mode dominant. The second is that the simplified procedure proposed in Section 3 can accurately estimate the seismic risk of isolated structures, again based on the same assumptions. This means that designers can size and select their isolation systems and evaluate them in terms of displacement-based risk quantities. It also means that the seismic performance of existing base isolation systems may be simply evaluated in the same way (i.e., risk of displacement-based failure of the device).

If the same process outlined above for the displacement threshold of $\Delta_{\text{lim}} = 0.4$ m is repeated and the MAFE at all displacement levels is computed, the demand-hazard curve shown in Figure 11 is obtained. This shows the risk of exceeding a given displacement threshold for a range of FPB device displacements. Designers may use such a curve to determine the risk of different displacements being exceeded for a particular FPB isolation in a given site location. More importantly, it shows how the proposed simplified method's estimate of MAFE across all displacement levels matches the actual risk computed via detailed analysis using numerical models and several ground motion records for each case study structure. This means that an excellent estimate of the risk of FPB device failure can be easily estimated using the proposed procedure with a fair degree of accuracy across all displacement levels and without any detailed knowledge of the superstructure's structural configuration. This is reflected in how the demand-hazard curves obtained from all case study structures are very similar, despite the notable differences in the superstructure's typology. There is a slight deviation at higher displacement values for the case of the six storey MRF system, likely due to its increased flexibility (Table 1). It is important to note that these case studies represent structural systems that are not explicitly designed to code requirements but are assumed to remain elastic. This approach was followed to keep the results generic and not specific to a particular building code or region. The results indicate that the proposed approach can simply estimate displacement-based risk in the isolator bearings. In practical application, however, the relevant building code regarding device properties, dimensions and also the superstructure design criteria must still be followed. More specific case studies could look to verify the results presented here.

## 5 | DISCUSSION

From the case study implementation and validation presented in previous sections, it is clear that the proposed procedure offers a simple and effective way of selecting FPB bearings as part of a risk-targeted seismic design or also the assessment of existing structures with isolators. However, it is important to note that it focuses entirely on the performance of the FPB device. The procedure and results presented strictly apply to single FPB with a uniform sliding surface, and the extension of such an approach to other types of friction-based isolators would need further investigation. In design, the overall performance of the building is of interest, meaning that the demand in the superstructure is also pertinent. The proposed procedure is not intended to be a comprehensive method for isolated structures but rather a dependable tool to ensure that the risk of device failure can be quantified and refined in an expedited manner, thus overcoming the main limitations of the methods currently[12,14–16] used. The complete seismic design of buildings must then still follow dynamic verification analysis of the whole building to verify other performance requirements (e.g., storey drift or floor accelerations). Still, a good starting design is always needed. In particular, the amount of base shear and accelerations transmitted to the superstructure may be problematic from a structural and non-structural perspective.[81] The magnitude of these quantities can be controlled by changing the device properties or the target device displacement limit. Future parametric studies can investigate the relations between these quantities to provide some prescriptive guidance. However, it is important to note that past studies[23–25,71] have looked at these excessive structural and non-structural demands and potential structural collapse generally under the assumption that the FPB device has exceeded its displacement capacity or has collided with the moat boundary wall. This is the type of problem that the proposed design procedure described here aims to directly protect against via sufficient risk mitigation. Other proposals[30,31] have focussed more on enhancing the device displacement capacity by a fixed ratio without full consideration of seismic hazard uncertainty,[82] which may not be ideal in the overall risk mitigation.[29]

In cases where the isolated building's superstructure demands cannot be adequately controlled, supplemental devices may be considered to ensure sufficient overall building performance. Devices such as passive dampers and active or semi-active control systems may be introduced. Past studies such as Zargar et al.[83,84] have experimentally investigated using a gap damper alongside an isolation system to reduce displacement demands. They found that while displacements were effectively reduced as intended, the floor accelerations in the superstructure tended to be amplified. Other similar approaches were trialled by De Domenico et al.[85,86] to reduce displacements and noted a reduction in the accelerations when different friction coefficient surfaces or shape memory alloy devices were utilised. Other kinds of isolator bearings, such as triple friction pendulums,[87] can offer advantages in terms of controlling the floor accelerations in the superstructure by providing a smoother backbone transition than that shown in Figure 1 via the use of multiple sliding surfaces.

Semi-active control systems[88] may also be considered as a potential solution to the multifaceted nature of limiting force and acceleration transmission to the superstructure of isolated structures. The flexible nature of these systems allows different objectives to be targeted and may prove to be a viable solution. Furthermore, they may also assist in situations where large near-fault pulses induce large displacement demands in the FPB devices. Other specialised devices to control unwanted superstructure behaviour have been devised and implemented in Japan also, with some systems focussing on moat wall buffers or combinations with rubber material and sliders, for example. This work shows that while the proposed risk-based procedure presented here provides an accurate means to control FPB device response and risk of failure, its combination with devices used to control other facets of the superstructure to maintain operability can be the focus of future work.

## 6 | SUMMARY AND CONCLUSIONS

This article has discussed the seismic design of single FPB isolation systems. It was seen how current design methods offered in building codes around the world focus on a trial-and-error intensity-based approach to verify FPB device suitability. This paper has developed a novel risk-based design methodology for FPB-isolated structures. It proposed a closed-form and simplified probabilistic approach to assess the risk of failure based on device displacement response by knowing just the site seismic hazard and the FPB device properties (i.e., dynamic friction coefficient and effective radius of curvature). A large parametric study was carried out to facilitate such a simplified method, and an empirical demand-intensity model characterising the seismic response of several FPB device combinations was developed. This was done using spectral acceleration at a period directly corresponding to that of the isolator response once activated since it was deemed a more suitable and efficient IM characterising FPB response.

The proposed risk-based methodology was described in detail and presented step-by-step to allow easy implementation in practice. A series of examples were tested whereby the displacement-based risk of failure was evaluated for a series of case study structures. These comprised both short and tall along with stiff and flexible structures to assess the method's capability for structural systems with different dynamic properties. The proposed method's ability to predict the mean annual frequency of exceeding, or risk of failing, a given displacement threshold was then evaluated against a more robust and computationally intensive approach. This involved the evaluation of the isolated structures' dynamic response via full numerical models at several seismic intensities using hazard-consistent ground motion record sets through MSA. These results evaluated the demand-intensity model's accuracy and the estimate of the risk of failure concerning a predefined displacement threshold. Regarding the demand-intensity model developed here, it was seen how the predicted median and dispersion of the fragility functions derived from MSA matched the predicted values from the demand-intensity models quite well. Furthermore, the risk was seen to be estimated with very high accuracy by the proposed method when compared to extensive analyses.

As a result of this work and its case study example, the following concluding points can be made:

- This proposed method means that designers can size and select their FPB isolation systems in a more risk-aware manner using a straightforward tool. This is also more direct than current design methods utilised in building codes worldwide that operate on a trial-and-error basis following numerical verification analyses. The proposed tool can be implemented in just a few simple steps and allows practitioners to have a very good first trial before conducting their verification analyses.
- Conversely, it also means that the risk of device failure (i.e., exceeding a known displacement threshold) in existing buildings in a given region can be quickly estimated to identify the isolated structures at an unacceptably high level of risk. Again, this is with the knowledge of just the FPB isolation system (i.e., no superstructure information is required) and without the need for any numerical analysis. This represents a powerful tool in the context of the regional assessment of such building typologies.
- While not considered here, other sources of device uncertainty (e.g., velocity or heating effects and impacts of a superstructure's higher mode contribution) can be further investigated to provide more quantifications and specific design guidance on how these aspects may be considered within such a simplified tool's approach.
- Future efforts may focus on further consideration of the overall building performance and how it can be handled in the context presented here. This includes the superstructure flexibility and possible non-linear behaviour and economic losses due to moat wall or isolator boundary collision. The work presented applies to low to mid-rise structures whose superstructure response is well-represented by first mode behaviour; its extension to taller buildings where the first mode response is less dominant should be examined further also.

## ACKNOWLEDGEMENTS

The work presented in this paper has been developed within the framework of the project "Dipartimenti di Eccellenza," funded by the Italian Ministry of Education, University and Research at IUSS Pavia.

## DATA AVAILABILITY STATEMENT

Data sharing is not applicable to this article as no new data were created or analysed in this study.

## ORCID

*Gerard J. O'Reilly* https://orcid.org/0000-0001-5497-030X
*Masayoshi Nakashima* https://orcid.org/0000-0002-3598-8560

## REFERENCES

1. Housner GW. Limit design of structures to resist earthquakes. *Proceedings of First World Conference on Earthquake Engineering* 1956.
2. Christopoulos C, Filiatrault A. *Principles of Passive Supplemental Damping and Seismic Isolation*. IUSS Press; 2006.
3. Kobori T, Koshika N, Yamada K, Ikeda Y. Seismic-response-controlled structure with active mass driver system. Part 1: design. *Earthq Eng Struct Dyn*. 1991;20(2):133-149. doi:10.1002/eqe.4290200204
4. Spencer BF, Nagarajaiah S. State of the art of structural control. *J Struct Eng*. 2003;129(7):845-856. doi:10.1061/(ASCE)0733-9445(2003)129:7(845)

5. Miranda E, Mosqueda G, Retamales R, Pekcan G. Performance of nonstructural components during the 27 february 2010 Chile earthquake. *Earthq Spectra*. 2012;28(S1):S453-S471. doi:10.1193/1.4000032
6. Shahnazaryan D, O'Reilly GJ, Monteiro R. Story loss functions for seismic design and assessment: development of tools and application. *Earthq Spectra*. 2021;37(4):2813-2839. doi:10.1177/87552930211023523
7. Kelly JM. Aseismic base isolation: review and bibliography. *Soil Dyn Earthquake Eng*. 1986;5(4):202-216. doi:10.1016/0267-7261(86)90006-0
8. Naeim F, Kelly JM. *Design of Seismic Isolated Structures: From Theory to Practice*. Wiley; 1999.
9. Zayas VA, Low SS, Mahin SA. A simple pendulum technique for achieving seismic isolation. *Earthq Spectra*. 1990;6(2):317-333. doi:10.1193/1.1585573
10. Zayas V, Low S, Mahin S. The FPS earthquake resistant system. *UCB/EERC Report*. 1987;87(01).
11. Calvi PM, Calvi GM. Historical development of friction-based seismic isolation systems. *Soil Dyn Earthquake Eng*. 2018;106:14-30. doi:10.1016/j.soildyn.2017.12.003
12. CEN. *Eurocode 8: Design of Structures for Earthquake Resistance - Part 1: General Rules, Seismic Actions and Rules for Buildings (EN 1998-1:2004)*. 2004.
13. CEN. *EN 15129:2018: Anti-seismic devices*. 2018.
14. NTC. *Norme Tecniche Per Le Costruzioni*. 2018.
15. ASCE 7–16. *Minimum Design Loads and Associated Criteria for Buildings and Other Structures*. 2016.
16. NZSEE. *Guideline for the Design of Seismic Isolation Systems for Buildings (Draft)*. 2019.
17. Higashino M, Okamoto S. *Response Control and Seismic Isolation of Buildings*. Routledge; 2006. doi:10.4324/9780203018866
18. Pan P, Zamfirescu D, Nakashima M, Nakayasu N, Kashiwa H. Base-isolation design practice in japan: introduction to the post-kobe approach. *J Earthquake Eng*. 2005;9(1):147-171.
19. Becker TC, Yamamoto S, Hamaguchi H, Higashino M, Nakashima M. Application of isolation to high-rise buildings: a Japanese design case study through a U.S. design code lens. *Earthq Spectra*. 2015;31(3):1451-1470. doi:10.1193/052813EQS136M
20. Kitayama S, Constantinou MC. Probabilistic seismic performance assessment of seismically isolated buildings designed by the procedures of ASCE/SEI 7 and other enhanced criteria. *Eng Struct*. 2019;179:566-582. doi:10.1016/j.engstruct.2018.11.014
21. Iervolino I, Spillatura A, Bazzurro P. Seismic reliability of code-conforming italian buildings. *J Earthquake Eng*. 2018;22(sup2):5-27. doi:10.1080/13632469.2018.1540372
22. Becker TC, Bao Y, Mahin SA. Extreme behavior in a triple friction pendulum isolated frame. *Earthq Eng Struct Dyn*. 2017;46(15):2683-2698. doi:10.1002/eqe.2924
23. Erduran E, Dao ND, Ryan KL. Comparative response assessment of minimally compliant low-rise conventional and base-isolated steel frames. *Earthq Eng Struct Dyn*. 2011;40(10):1123-1141. doi:10.1002/eqe.1078
24. Pant DR, Wijeyewickrema AC. Performance of base-isolated reinforced concrete buildings under bidirectional seismic excitation considering pounding with retaining walls including friction effects. *Earthq Eng Struct Dyn*. 2014;43(10):1521-1541. doi:10.1002/eqe.2409
25. Masroor A, Mosqueda G. Assessing the collapse probability of base-isolated buildings considering pounding to moat walls using the FEMA P695 methodology. *Earthq Spectra*. 2015;31(4):2069-2086. doi:10.1193/092113EQS256M
26. Bao Y, Becker TC. Inelastic response of base-isolated structures subjected to impact. *Eng Struct*. 2018;171:86-93. doi:10.1016/j.engstruct.2018.05.091
27. Takayama M. Brief report of seismically isolated buildings in 2016 Kumamoto Earthquake. *Bucharest Seminar on Seismic Isolation, Technical University of Civil Engineering Bucharest*. 2016.
28. Cornell CA, Jalayer F, Hamburger RO, Foutch DA. Probabilistic basis for 2000 SAC federal emergency management agency steel moment frame guidelines. *J Struct Eng*. 2002;128(4):526-533. doi:10.1061/(ASCE)0733-9445(2002)128:4(526)
29. Kazantzi AK, Vamvatsikos D. Practical performance-based design of friction pendulum bearings for a seismically isolated steel top story spanning two RC towers. *Bull Earthquake Eng*. 2021;19:1231-1248. doi:10.1007/s10518-020-01011-x
30. Kitayama S, Constantinou MC. Collapse performance of seismically isolated buildings designed by the procedures of ASCE/SEI 7. *Eng Struct*. 2018;164:243-258. doi:10.1016/j.engstruct.2018.03.008
31. Zayas VA, Mahin SA, Constantinou MC. Seismic isolation standard for continued functionality. *UCB/SEMM-2017/03*. 2017.
32. Günay S, Mosalam KM. PEER performance-based earthquake engineering methodology, revisited. *J Earthquake Eng*. 2013;17(6):829-858. doi:10.1080/13632469.2013.787377
33. Furinghetti M, Yang T, Calvi PM, Pavese A. Experimental evaluation of extra-stroke displacement capacity for Curved Surface Slider devices. *Soil Dyn Earthquake Eng*. 2021;146:106752. doi:10.1016/j.soildyn.2021.106752
34. Cornell CA, Krawinkler H. Progress and challenges in seismic performance assessment. *PEER Center News*. 2000;3(2):1-2.
35. Fenz DM, Constantinou MC. *Mechanical Behavior of Multi-Spherical Sliding Bearings*. 2008.
36. Mollaioli F, Lucchini A, Cheng Y, Monti G. Intensity measures for the seismic response prediction of base-isolated buildings. *Bull Earthquake Eng*. 2013;11(5):1841-1866. doi:10.1007/s10518-013-9431-x
37. Ryan KL, Chopra AK. Estimating the seismic displacement of friction pendulum isolators based on non-linear response history analysis. *Earthq Eng Struct Dyn*. 2004;33(3):359-373. doi:10.1002/eqe.355
38. Ryan KL, Chopra AK. Estimation of seismic demands on isolators based on nonlinear analysis. *J Struct Eng*. 2004;130(3):392-402. doi:10.1061/(ASCE)0733-9445(2004)130:3(392)
39. Kohrangi M, Bazzurro P, Vamvatsikos D. Vector and scalar IMs in structural response estimation: part II – building demand assessment. *Earthq Spectra*. 2016;32(3):1525-1543. doi:10.1193/053115EQS081M

40. Kazantzi AK, Vamvatsikos D. Intensity measure selection for vulnerability studies of building classes. *Earthq Eng Struct Dyn*. 2015;44(15):2677-2694. doi:10.1002/eqe.2603
41. Eads L, Miranda E, Lignos DG. Average spectral acceleration as an intensity measure for collapse risk assessment. *Earthq Eng Struct Dyn*. 2015;44(12):2057-2073. doi:10.1002/eqe.2575
42. Dávalos H, Miranda E. Filtered incremental velocity: a novel approach in intensity measures for seismic collapse estimation. *Earthq Eng Struct Dyn*. 2019;48(12):1384-1405. doi:10.1002/eqe.3205
43. O'Reilly GJ. Limitations of Sa(T1) as an intensity measure when assessing non-ductile infilled RC frame structures. *Bull Earthquake Eng*. 2021;19(6):2389-2417. doi:10.1007/s10518-021-01071-7
44. O'Reilly GJ. Seismic intensity measures for risk assessment of bridges. *Bull Earthquake Eng*. 2021;19(9):3671-3699. doi:10.1007/s10518-021-01114-z
45. O'Reilly GJ, Calvi GM. Quantifying seismic risk in structures via simplified demand–intensity models. *Bull Earthquake Eng*. 2020;18(5):2003-2022. doi:10.1007/s10518-019-00776-0
46. O'Reilly GJ, Monteiro R. Probabilistic models for structures with bilinear demand-intensity relationships. *Earthq Eng Struct Dyn*. 2019;48(2):253-268. doi:10.1002/eqe.3135
47. Romão X, Delgado R, Costa A. Alternative closed-form solutions for the mean rate of exceedance of structural limit states. *Earthq Eng Struct Dyn*. 2013;42(12):1827-1845. doi:10.1002/eqe.2300
48. Veletsos AS, Newmark NM. Effect of inelastic behavior on the response of simple systems to earthquake motions. *Proceedings of the third world conference on earthquake engineering*, 1960.
49. Vidic T, Fajfar P, Fischinger M. Consistent inelastic design spectra: strength and displacement. *Earthq Eng Struct Dyn*. 1994;23(5):507-521. doi:10.1002/eqe.4290230504
50. Dolšek M, Fajfar P. Inelastic spectra for infilled reinforced concrete frames. *Earthq Eng Struct Dyn*. 2004;33(15):1395-1416. doi:10.1002/eqe.410
51. Miranda E. Inelastic displacement ratios for structures on firm sites. *J Struct Eng*. 2000;126(10):1150-1159. doi:10.1061/(ASCE)0733-9445(2000)126:10(1150)
52. Vamvatsikos D, Cornell CA. Direct estimation of the seismic demand and capacity of MDOF systems through Incremental Dynamic Analysis of an SDOF approximation. *J Struct Eng*. 2005;131(4):589-599.
53. Nafeh AMB, O'Reilly GJ, Monteiro R. Simplified seismic assessment of infilled RC frame structures. *Bull Earthquake Eng*. 2020;18(4):1579-1611. doi:10.1007/s10518-019-00758-2
54. Freeman SA. The capacity spectrum method as a tool for seismic design. *11th European Conference of Earthquake Engineering*, 1998.
55. Jacobsen LS. Steady forced vibration as influencd by damping. *Transactions of ASME*. 1930;52(15):169-181.
56. Dwairi HM, Kowalsky MJ, Nau JM. Equivalent damping in support of direct displacement-based design. *J Earthquake Eng*. 2007;11(4):512-530. doi:10.1080/13632460601033884
57. Priestley MJN, Calvi GM, Kowalsky MJ. *Displacement Based Seismic Design of Structures*. IUSS Press; 2007.
58. Wijesundara KK, Nascimbene R, Sullivan TJ. Equivalent viscous damping for steel concentrically braced frame structures. *Bull Earthquake Eng*. 2011;9(5):1535-1558. doi:10.1007/s10518-011-9272-4
59. O'Reilly GJ, Sullivan TJ. Direct displacement-based seismic design of eccentrically braced steel frames. *J Earthquake Eng*. 2016;20(2):243-278. doi:10.1080/13632469.2015.1061465
60. Grant D, Blandon CA, Priestley MJN. *Modelling Inelastic Response in Direct Displacement Based Design*. 2005.
61. McKenna F, Scott MH, Fenves GL. Nonlinear finite-element analysis software architecture using object composition. *J Comput Civil Eng*. 2010;24(1):95-107. doi:10.1061/(ASCE)CP.1943-5487.0000002
62. Calvi GM, Ceresa P, Casarotti C, Bolognini D, Auricchio F. Effects of axial force variation in the seismic response of bridges isolated with friction pendulum systems. *J Earthquake Eng*. 2004;8(sup001):187-224. doi:10.1080/13632460409350525
63. Kumar M, Whittaker AS, Constantinou MC. Extreme earthquake response of nuclear power plants isolated using sliding bearings. *Nucl Eng Des*. 2017;316:9-25. doi:10.1016/j.nucengdes.2017.02.030
64. Jalayer F, Ebrahimian H, Miano A, Manfredi G, Sezen H. Analytical fragility assessment using unscaled ground motion records. *Earthq Eng Struct Dyn*. 2017;46(15):2639-2663. doi:10.1002/eqe.2922
65. Ancheta TD, Darragh RB, Stewart JP, et al. NGA-West2 database. *Earthq Spectra*. 2014;30(3):989-1005. doi:10.1193/070913EQS197M
66. Vamvatsikos D, Cornell CA. Incremental dynamic analysis. *Earthq Eng Struct Dyn*. 2002;31(3):491-514. doi:10.1002/eqe.141
67. Dávalos H, Miranda E. Evaluation of the scaling factor bias influence on the probability of collapse using S a (T 1) as the intensity measure. *Earthq Spectra*. 2019;35(2):679-702. doi:10.1193/011018EQS007M
68. Jalayer F, Cornell CA. Alternative non-linear demand estimation methods for probability-based seismic assessments. *Earthq Eng Struct Dyn*. 2009;38(8):951-972. doi:10.1002/eqe.876
69. FEMA, ATC. *Quantification of Building Seismic Performance Factors*. 2009. doi:10.1016/j.compstruc.2009.08.001
70. FEMA. *FEMA P-58-1: Seismic Performance Assessment of Buildings*. 2018.
71. Kitayama S, Constantinou MC. Effect of displacement restraint on the collapse performance of seismically isolated buildings. *Bull Earthquake Eng*. 2019;17(5):2767-2786. doi:10.1007/s10518-019-00554-y
72. Barone S, Calvi GM, Pavese A. Experimental dynamic response of spherical friction-based isolation devices. *J Earthquake Eng*. 2019;23(9):1465-1484. doi:10.1080/13632469.2017.1387201

73. Vamvatsikos D. Derivation of new SAC/FEMA performance evaluation solutions with second-order hazard approximation. *Earthq Eng Struct Dyn*. 2013;42(8):1171-1188. doi:10.1002/eqe.2265
74. Woessner J, Laurentiu D, Giardini D, et al. The 2013 European Seismic Hazard Model: key components and results. *Bull Earthquake Eng*. 2015;13(12):3553-3596. doi:10.1007/s10518-015-9795-1
75. GEM. The OpenQuake Engine User Instruction Manual 2019: 189. doi:10.13117/GEM.OPENQUAKE.MAN.ENGINE.3.7.1
76. Tsai KC, Popov EP. Steel Beam-Column Joints in Seismic Moment Resiting Frames. *EERC Report No UCB/EERC/88-19* 1988.
77. Lin T, Haselton CB, Baker JW. Conditional spectrum-based ground motion selection. Part I: hazard consistency for risk-based assessments. *Earthq Eng Struct Dyn*. 2013;42(12):1847-1865. doi:10.1002/eqe.2301
78. Franchin P, Ragni L, Rota M, Zona A. Modelling uncertainties of italian code-conforming structures for the purpose of seismic response analysis. *J Earthquake Eng*. 2018;22(sup2):1964-1989. doi:10.1080/13632469.2018.1527262
79. O'Reilly GJ, Sullivan TJ. Quantification of modelling uncertainty in existing Italian RC frames. *Earthq Eng Struct Dyn*. 2018;47(4):1054-1074. doi:10.1002/eqe.3005
80. Liel AB, Haselton CB, Deierlein GG, Baker JW. Incorporating modeling uncertainties in the assessment of seismic collapse risk of buildings. *Struct Saf*. 2009;31(2):197-211. doi:10.1016/j.strusafe.2008.06.002
81. Shahnazaryan D, O'Reilly GJ, Monteiro R. On the seismic loss estimation of integrated performance-based designed buildings. *Earthq Eng Struct Dyn*. 2022. doi:10.1002/eqe.3638
82. Baker J, Bradley B, Stafford P. *Seismic Hazard and Risk Analysis*. Cambridge University Press; 2021. doi:10.1017/9781108425056
83. Zargar H, Ryan KL, Rawlinson TA, Marshall JD. Evaluation of a passive gap damper to control displacements in a shaking test of a seismically isolated three-story frame. *Earthq Eng Struct Dyn*. 2017;46(1):51-71. doi:10.1002/eqe.2771
84. Zargar H, Ryan KL, Marshall JD. Feasibility study of a gap damper to control seismic isolator displacements in extreme earthquakes. *Struct Control Health Monit*. 2013;20(8):1159-1175. doi:10.1002/stc.1525
85. De Domenico D, Gandelli E, Quaglini V. Effective base isolation combining low-friction curved surface sliders and hysteretic gap dampers. *Soil Dyn Earthquake Eng*. 2020;130:105989. doi:10.1016/j.soildyn.2019.105989
86. De Domenico D, Gandelli E, Quaglini V. Adaptive isolation system combining low-friction sliding pendulum bearings and SMA-based gap dampers. *Eng Struct*. 2020;212:110536. doi:10.1016/j.engstruct.2020.110536
87. Fenz DM, Constantinou MC. Modeling triple friction pendulum bearings for response-history analysis. *Earthq Spectra*. 2008;24(4):1011-1028. doi:10.1193/1.2982531
88. Kurata N, Kobori T. Reliability of Applied semiactive structural control system. *J Struct Eng*. 2003;129(7):914-921. doi:10.1061/(ASCE)0733-9445(2003)129:7(914)


**How to cite this article:** O'Reilly GJ, Yasumoto H, Suzuki Y, Calvi GM, Nakashima M. Risk-based seismic design of base-isolated structures with single surface friction sliders. *Earthquake Engng Struct Dyn*. 2022;1–21. https://doi.org/10.1002/eqe.3668